Characterization of mass transport deposits using seismic attributes: Upper Leonard Formation, Permian Basin

Paritosh Bhatnagar[1], Sumit Verma[1], and Ron Bianco[2]

Abstract

The Permian Basin is a structurally complex sedimentary basin with an extensive history of tectonic deformation. As the basin evolved through time, sediments dispersed into the basin floor from surrounding carbonate platforms leading to various mass movements. One such mass movement is observed on a 3D seismic survey in the Upper Leonard interval (Lower Permian) of the Midland Basin that is characteristic of a mass transport deposit (MTD). The 350 ft thick MTD mapped in the study area is 5 mi wide, extends up to 14 mi basinward, and covers only the translational and compressional regime of the mass movement. A unique sedimentary feature, unlike those observed previously, is mapped and interpreted as gravity spreading. MTDs have been extensively studied in the Delaware Basin of Permian-aged strata; however, only a few works have been published on the geomorphological expression of MTDs using seismic and seismic attributes to delineate the shape, size, and anatomy of this subsurface feature. The MTD in the study area exhibits an array of features including slide, slump, basal shear surface, and MTD grooves. In cross section, the MTD is characterized as chaotic with semitransparent reflectors terminating laterally against a coherent package of seismic facies, or the lateral wall. Sobel filter-based coherence, structural curvature, dip magnitude, and dip azimuth attributes are used to map thrust faults within the discontinuous MTD. Kinematic evidence provided by the Upper Spraberry isopach suggests that this MTD was sourced north of the Midland Basin and deposited on the basin floor fairway. Slope strata are interpreted from well-log analysis showing MTD as a mixture of carbonates and siliciclastics with a moderate to high resistivity response.

Introduction

Mass movements generate the most impressive deposits in terms of volume on the earth's surface in subaqueous and subaerial settings. Nissen et al. (1999) are the first to document the various aspects of mass movements in seismic data using coherence attribute in the Nigerian continental slope including mass transport deposits (MTDs). Such mass movements are distinctive in deepwater depositional systems mostly due to their large size, geomorphology, and chaotic internal character (Shipp et al., 2011). Furthermore, MTDs have been known to play a significant role in petroleum exploration because they may be top and lateral seals or may have acted as paleobathymetric constraints on the deposition of overlying reservoir deposits (Amerman, 2009). Regardless of their architecture or their ability to hold hydrocarbons, MTDs are in essence earth's modern and ancient deepwater stratigraphic record and are an important tool in our understanding of mass movements in slope settings around the world.

At the time of MTD deposition, the Midland Basin was surrounded by carbonate platforms, which provided vast inputs of carbonates into the basin. The Leonardian Series (Lower Permian) had shelf to open marine depositional environments in the Midland Basin, which included siliciclastic and carbonate rocks with detrital limestone restricted to slope and base-of-slope settings (Hamlin and Baumgardner, 2013). Handford (1981a) points out that the Leonardian-aged sediments (Spraberry Formation) were deposited as a large basin-floor submarine fan system and are commonly interpreted as deposits of turbidity currents and debris flow. The present study observed a different spectrum of mass movement on 3D seismic in the Upper Leonard interval, which is representative of MTDs. In this study, an MTD is described as a gravity-flow deposit in which grains remain in contact with each other as opposed to turbidity deposits.

The Permian Basin has been known to host vast amounts of mass movements, and studies have been conducted to understand the importance of the underlying paleobathymetry and its effect on sediment flow and reservoir facies distribution. Amerman (2009) investigates the structure and stratigraphy of deepwater MTDs in the Permian Cutoff Formation and overlying Brushy

[1]UT Permian Basin, Department of Geosciences, Odessa, Texas, USA. E-mail: paritoshb12@gmail.com; sumit.verma.geophysicist@gmail.com; verma_s@utpb.edu.

[2]Fasken Oil and Ranch Ltd, Midland, Texas, USA. E-mail: ronb@forl.com.

Manuscript received by the Editor 12 March 2019; published ahead of production 30 July 2019.

This paper appears in *Interpretation*, Vol. 7, No. 4 (November 2019); p. 1–14, 19 FIGS.

http://dx.doi.org/10.1190/INT-2019-0036.1.

Canyon Formation in the Delaware Basin to analyze the internal architecture and stratigraphic relationship of MTDs in succession. Allen et al. (2013) study MTD in the second Bone Spring Formation in the Delaware Basin of West Texas, USA, in which the authors use seismic and well-log data to map the compressional features of the MTD along with the log responses to highlight the MTDs reservoir potential. Asmus and Grammer (2013) further investigate the architectural attributes of less than 3 ft thick turbidites and MTDs in the Delaware Basin of the Upper Bone Spring Formation. Based on their study on two cored wells, the authors conclude that more than 90% of MTDs (slumps and debris flows) observed in the cores are easily identified in image logs. Moreover, the MTDs were correlated to decreasing gamma-ray and increasing resistivity responses in conventional logs. In summary, several extensive studies conducted in the Delaware Basin highlight the importance of paleobathymetry and the subscale architecture and composition exhibited by MTDs.

Even though mass movements have been well-documented in the lower Permian period, few works have been conducted to illustrate the geomorphology of these features using seismic expression. In this paper, we first review the geology of the Upper Leonard interval of the Midland Basin and understand the paleobathymetry of the Upper Spraberry Formation and its control on the morphology of the overlying MTD. Then, we move from available seismic data to detailed analysis of characterizing the MTD using seismic attributes, and we conclude with the overall interpretation of the shape, size, and anatomy of this subsurface feature. With integrated well control and 3D seismic data, new insights are put forward in our understanding of how paleobathymetry affect sediment flow and unfold the geologic evolution of the MTD mapped in the study area.

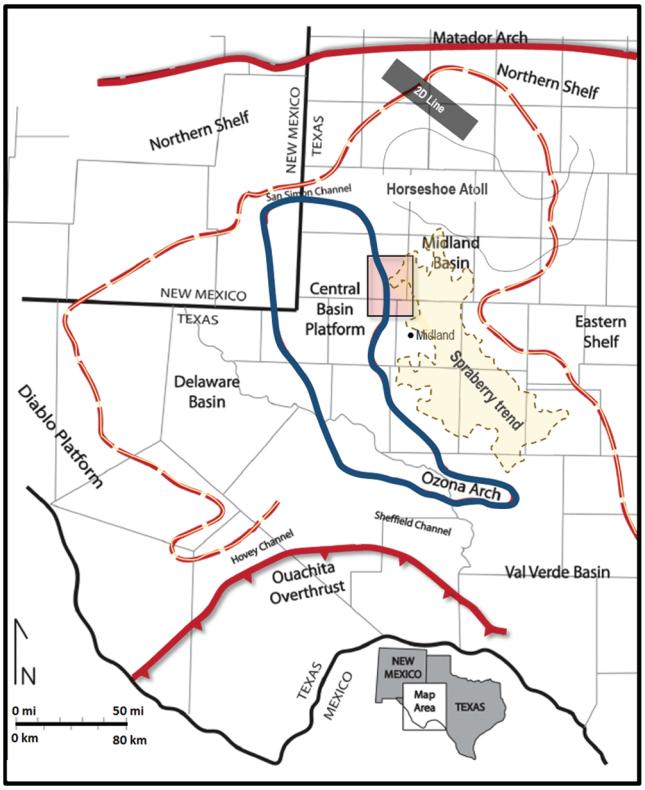

Figure 1. Paleogeography of the Permian Basin in early Permian time showing study area in the red box (modified from Ruppel et al., 2000). The blue polygon highlights the outline of the Central Basin Platform, and the dashed red/yellow line highlights the shelf edge.

Geology of the study area

The extent of the Permian Basin spans an area of approximately 250 mi wide and 300 mi long in West Texas and Southeastern New Mexico of the United States. Before the Permian Basin completely formed, it was first described to be a shallow marine, slightly dipping basin referred to as the Tobosa Basin (Hoak et al., 1998). It was not until the upper Paleozoic time (Late Mississippian — Early Pennsylvanian) when the North American plate collided with the South American plate giving rise to the Marathon Ouachita Orogeny (Figure 1). This massive compressional event gave rise to the Central Basin Platform (a northwest-trending uplifted basement block) bounded by the Delaware Basin (to the west) and the Midland Basin (to the east; Kelly et al., 2012). The MTD mapped in this study using seismic was observed in the Upper Leonard interval of the Midland Basin, which lies in the Leonardian series of the Permian-aged strata (Figure 2).

The Leonardian stratigraphy in the Midland Basin records deposition in an intracratonic deepwater basin, bounded by shallow-water carbonate platforms. Sea-level

STRATIGRAPHIC CHART

System	Series	Central Basin Platform	Midland Basin
PERMIAN	GUADALUPIAN	TANSILL	TANSILL
		YATES	YATES
		7 RIVERS	7 RIVERS
		QUEEN	QUEEN
		GRAYBURG	GRAYBURG
		SAN ANDRES	SAN ANDRES
	LEONARDIAN	GLORIETA	U. LEONARD
			U. SPRABERRY
		U. CLEARFORK	L. SPRABERRY
		TUBB	DEAN
		L. CLEARFORK	L. CLEARFORK
	WOLFCAMP	WOLFCAMP	WOLFCAMP

Figure 2. A simplified stratigraphic chart correlating the shelf to basin facies (modified from Handford, 1981a). The red box indicates the stratigraphic interval in which the MTD was deposited.

fluctuations controlled sediment input into the basin by flooding or exposing the platform. Slope environments, which separate the basin floor from surrounding shallow-water platforms, are characterized by abrupt stratigraphic discontinuities, detrital carbonates, and clinoformal geometries (Hamlin and Baumgardner, 2013). This is evident in Figure 3, which shows an interpreted regional 2D line trending northwest–southeast from the Northern shelf into the Midland Basin illustrating the prograding carbonate platform (clinoformal geometries) basinward due to continuous sea-level fall.

The Upper Leonardian interval in which the MTD deposited conforms on top of the Upper Spraberry Formation and is equivalent to the Glorietta Formation (Figure 2) on the platforms (Handford, 1981a, 1981b). Therefore, understanding the paleobathymetry of the underlying Spraberry Formation with the help of an isopach map can provide useful information on how the sediments were dispersed on the basin floor and how the underlying seabed exerted control on the morphology of the overlying MTD.

Regional mapping of the 1000 ft thick Spraberry fan cone shows that the fan system was deposited in water depths of 600–1000 ft (Handford, 1981a, 1981b). Basin-wide maps of sandstone distribution in the broadly defined lower and upper Spraberry clastic members (Handford, 1981a, 1981b) show that the principal sediment sources lay to the northwest, north, and northeast. This is evident in the Upper Spraberry isopach map, which shows depocenters around the Horseshoe Atoll in the north indicating probable entry points (Figure 4). The Horseshoe Atoll is an isolated carbonate platform in the northern Midland Basin that began in the Pennsylvanian as a broad carbonate buildup and was surrounded by basinal environments (Vest, 1970). By the Early Permian, more than 1000 ft of relief had developed on the aggrading platform system. Starting in the Wolfcampian and continuing through the Leonardian, the Horseshoe Atoll was buried by deep-water siliciclastic sediments. However, the differential compaction of sediment overlying the peak-and-saddle morphology of the Horseshoe Atoll influenced the

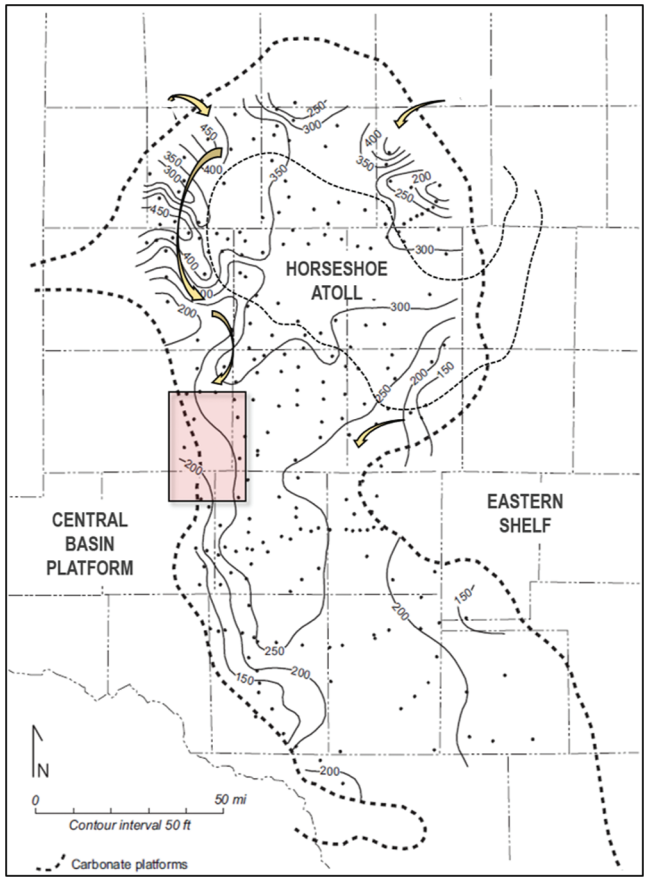

Figure 4. Isopach map of the Upper Spraberry interval. Arrows indicate the primary sediment flow into the basin during the time of deposition (redrawn from Handford 1981a, 1981b). The dots are the well control points for this isopach map. The study area is within the red box.

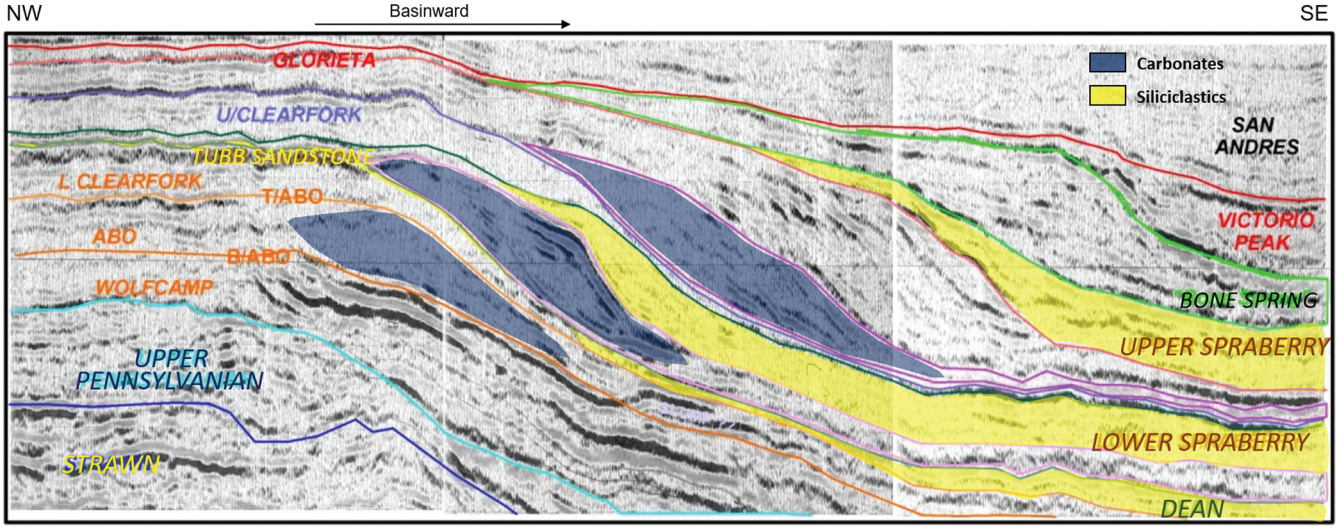

Figure 3. Interpreted regional 2D line trending northwest–southeast illustrating the prograding carbonate platform basinward due to forced regression (modified from Bhatnagar, 2018). See Figure 1 for approximate location.

sedimentation patterns of the upper Spraberry Formation. The toe of shelf slope also influenced paths of sediment transport, particularly for sediment entering the basin from the principal northwest sediment entry point. Wireline correlations (Ruppel et al., 2000) indicate that cyclic Leonardian platform deposits started prograding toward the basin into massive, clinoformal carbonates on the slope, which in turn, grade into flat-lying calcareous and siliciclastic intervals.

Available data

The C Ranch 3D prestack time migrated (PSTM) mega-merged seismic survey covers parts of Andrews, Ector, Midland, and Martin Counties with a seismic outline of approximately 400 mi^2 (Figure 1). All of the seismic surveys were acquired with vibroseis with a sweep of 8–90 Hz, a 2 ms sample rate, and processed with a bin size of 110 × 110 ft. Seismic data quality varies within the megamerged survey, due to the difference in the nominal fold and maximum offset of the surveys (Verma et al., 2013). The vertical resolution (one-fourth of a wavelength) for the mapped MTD is approximately 109 ft (33 m). We used three wells available in the study area to understand the MTDs' lithologic composition. The wireline logs were selected on the basis of log quality, resolution, and depth of penetration in the area of interest. Conventional wireline logs used include gamma ray, caliper log, shallow and deep resistivity, neutron porosity, and density porosity logs. Seismic synthetics were generated to tie in well logs to seismic. We picked the top and base of the MTD on a low-gamma-ray/high-resistivity-log response based on the correlation of the log signature with the MTD seismic reflectors.

MTD classification, processes, and morphology

Mass movements represent the main mechanism of sediment transport in deepwater settings and can range from inches to several miles in dimension. The term MTD includes only those processes in which sediments are moved *en masse* (i.e., grains do not move freely with respect to others) under the influence of gravity and nonfluid turbulence is the primary grain support mechanism. Thus, turbidity currents and other noncohesive flows are excluded (Asmus and Grammer, 2013). Even though MTDs are considered separate from turbidites, it should be recognized that a single depositional event can generate both types of deposits because they are part of the same depositional process. Hence, one process may evolve into another with time, or one depositional process may trigger the other.

Posamentier (2017) points out that one can determine whether one is in a deepwater setting from seismic data by looking for the presence of widespread polygonal faulting (i.e., shrinkage cracks), sediment waves, seismically resolvable MTDs, and the presence of clinoforms defining the deepwater setting (geomorphology). On seismic, MTDs have characteristic, stratigraphic, and geomorphologic features: basal linear grooved and scoured surfaces, hummocky relief at the top, and chaotic seismic facies, with internal thrust faulting being common (Posamentier and Martinsen, 2010).

The different processes comprising an MTD can be diverse (slide, slump, and debris flow) with varying degree of internal deformation of the sediments. Figure 5 shows a range of mass movements from slide/slump to increasingly turbulent movement of grains (turbidity flow). Slide/slump exhibits elastoplastic behavior and is moderately lithified as opposed to turbidite flows, which move almost entirely independently of other grains (fluidal behavior). The origin of these mass movements can be attributed to slope instability due to reactivation of preexisting extensional faults, fluctuations in sea level, and/or dissociation of gas hydrates, which is closely related to the shear strength of sediments (Festa et al., 2016). Hence, the type of deposit (creep, slide, and slump or debris flow) to be expected depends on the slope gradient, the resulting sediment velocity, and the hydrostatic forces between the sediment and fluid. Due to a low slope gradient, the processes that comprise the MTD observed in the Midland Basin are restricted to slides and slumps.

Slide and slumps

Slides involve the movement of sediments with little to no internal deformation and exhibit a laminar flow throughout the body of the sediment. This is accompanied by translation and/or folding of the sediments as they experience shear failure along a basal deformed zone (Moscardelli et al., 2006; Amerman, 2009). Slumps, on the other hand, are characterized by significant internal deformation leading to imbricate zone geometries (Lewis, 1971; Dingle, 1977) and are usually associated with the toe of slope region. The main fold type observed in a slump is the sheath fold formed by simple shear, and it experiences a main phase of plastic/ductile deformation in which folds are formed, followed by a late brittle phase when faults form (Martinsen, 1994).

Looking at the entire regime of the MTD, the upslope region is concave downslope and exhibits extensional faulting (Figure 6). The middle region is mainly transitional and most likely not deformed. The terminus or toe region is usually dominated by compressional deformation that produces thrust faults (Martinsen and Bakken, 1990; Posamentier and Walker, 2006). Submarine mass transport complexes on the modern seafloor often display complex rugosity on their upper surfaces along with detached folds and faults.

Mass transport morphology

MTDs can assume a variety of shapes and sizes ranging from lobate to sheet to channel (Posamentier et al., 2000; Posamentier and Kolla, 2003). The lobes can have steep flanks of up to 20°–30°, suggesting a flow mechanism that involved an abrupt halt and forming low-angle thrust faults as it comes in contact with and presses against the terminal wall (Figure 7). Sediments close to the terminal wall have presumably traveled the shortest distance (Posamentier and Martinsen, 2010). The

thrust faults are characterized as listric curvature, which originate at the base and extend through the top of the deposit orientated perpendicular to the flow direction (Posamentier and Martinsen, 2010). The striking linearity of grooves that are commonly observed at the base of MTDs form because of the laminar rather than turbulent flow that characterizes these flows.

Figure 8 shows a seismic cross section from the Bone Spring Formation (Leonardian) of the Delaware Basin where the deformed section is characterized by arcuate thrust faults dipping northwest (Allen et al., 2013). The MTD base acts as a detachment surface evidenced by coherent seismic reflector. The overlying strata above the MTD follow similar architecture indicating the MTD is bounded by an interval of approximately 400 ft. The log signature of the high- and low-resistivity responses in the deformed MTD zone agrees with the results presented by Asmus and Grammer (2013). Another recent study (Adiletta et al., 2019) conducted in the Delaware Basin has mapped the pressure ridges in a mass transport complex flowing from west to east during the Avalon (Leonardian) deposition (Figure 9). Studies such as those mentioned above provide great insight on how the basin evolved as the sediments were deposited on either side of the basin at a similar stratigraphic interval.

The internal chaotic nature of MTDs can sometimes be hard to interpret on seismic profiles because of their highly disruptive pattern. To overcome this problem, analysis of the seismic profile along with seismic attributes can be the optimum method to properly characterize the MTD's internal architecture. Ultimately with

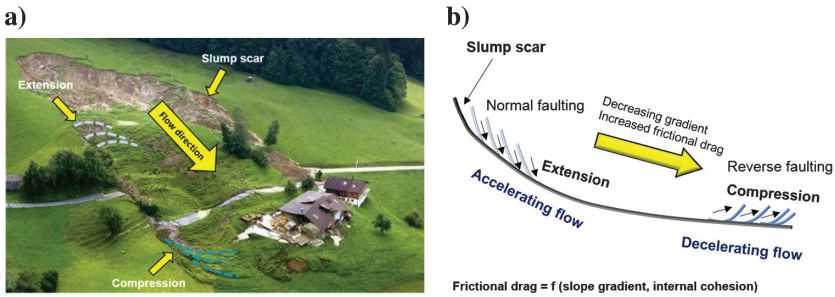

Figure 6. (a) A small MTD observed in the Austrian Alps and (b) compression and extension associated with MTD. Modified after Posamentier (2017).

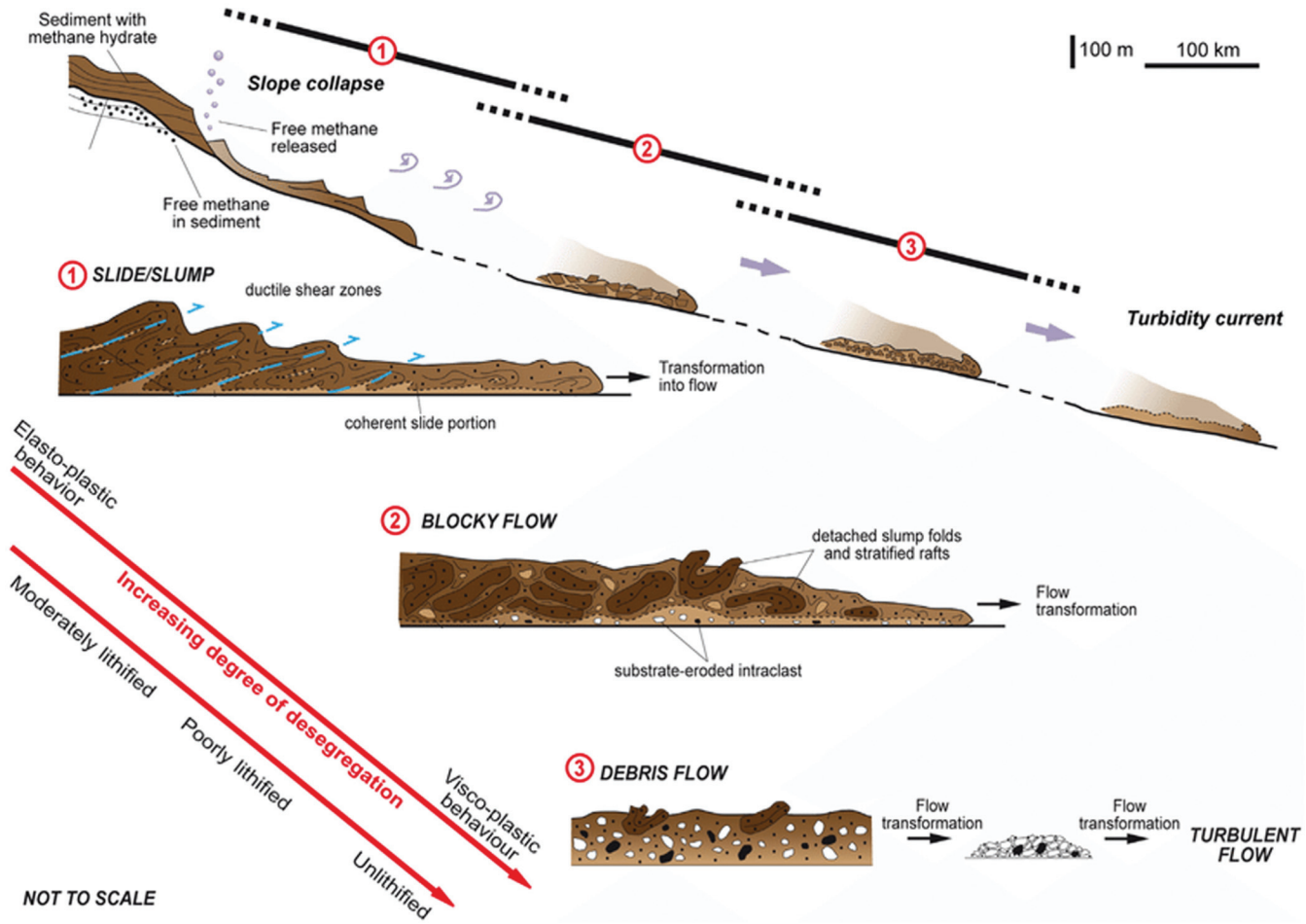

Figure 5. Different processes responsible for MTDs (modified from Festa et al., 2016). Blocky flow deposits represent a transitional zone between slump and debris flow deposits.

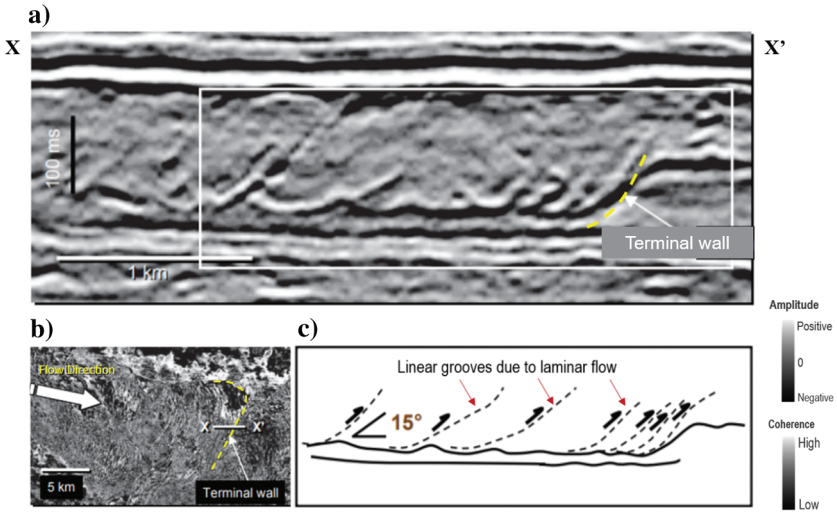

Figure 7. (a) Seismic cross section XX′, (b) coherency slice, and (c) interpreted line diagram showing the steeply dipping flanks. The large arrow indicates the direction of sediment flow (modified after Posamentier and Martinsen, 2010).

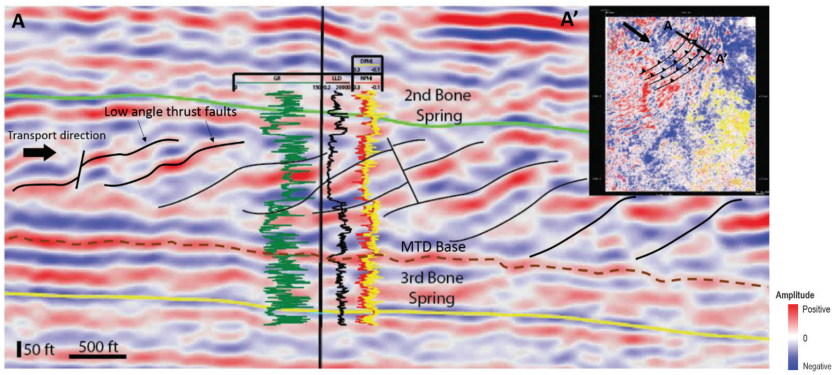

Figure 8. Section view characterizing the chaotic internal reflectors of the 400 ft MTD observed in the Delaware Basin (modified after Allen et al., 2013).

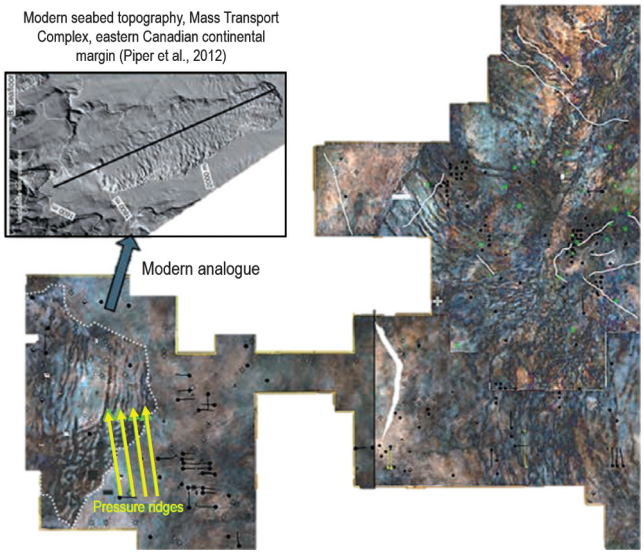

Figure 9. Avalon depositional environment highlighting mass movements revealed by spectral decomposition in the Delaware Basin (Adiletta et al., 2019).

proper well control and seismic coverage, it is possible to identify sweet spots if any within the MTD system.

Characterization of MTD using seismic attributes

The 3D seismic attributes are quantitative measures or derivative product (Marfurt, 2018) that provides insight on the external and internal geomorphology of geologic features. There are several attributes that can be used to map discontinuous features; however, geometric attributes are the most useful methodology for studying MTDs (Martinez, 2010). The MTD mapped in the study area covers only the translational and compressional regime of the mass movement, is lobate in shape, 5 miles wide, and extends up to 14 miles basinward. The following sections discuss how seismic attributes are used to help bring out certain geologic anomalies along with their interpretation to compartmentalize the MTD.

Seismic amplitude

Seismic amplitude is a quick and easy way to look at stratigraphic features without involving strenuous attribute calculations. Seismic amplitude is a measure of the change in impedance (product of density and velocity) of adjacent rock layers. For a picked Upper Leonard horizon, amplitudes values were extracted and viewed to understand the MTD geometry. Figure 10 shows a snapshot through time of how the amplitude anomalies map out going up the MTD stratigraphic section. The sinusoidal path taken by the sediments in the first MTD succession can be observed (Figure 10a), which highlights the translational regime of the mass movement. The imbricate thrust faults toward the compressional regime are hard to discern using amplitude values only. In general, impedance change can be inferred from the low- and high-amplitude anomalies but the plan view does not help much in characterizing the external morphology of the MTD.

Sobel filter (coherence)

The Sobel filter is an edge-detection technology that is commonly used in image processing packages; it scans the data horizontally and vertically to highlight discontinuities. The Sobel filter involves the computation of inline and crossline amplitude derivatives normalized by the energy. It detects breaks in the reflector configuration or lateral changes in the amplitude values and waveform shape and provides enhanced

image of small-scale geologic features, which helps in understanding the internal complexity of sedimentary features (Qi et al., 2017).

The discontinuous linear grooves observed within the MTD are thrust faults represented by low coherence values (Figure 11) caused by compressional forces as discussed by Posamentier and Martinsen (2010). Because the grooves are oriented in the overall north direction, it is interpreted that the sediments must be coming in from north (thrust faults align perpendicular to the sediment flow). The upper Spraberry isopach map further confirms this regional sediment flow direction. Although within the MTD, the direction of sediment movement can vary due to localized internal kinematics and seabed topography. The attribute further delineates the presence of lateral wall and the sinusoidal path (interpreted as MTD grooves) the sediments take before settling down. Sobel filter-based coherence gives a detailed aerial view of the overall lobate shape of the MTD. With the help of seismic section lines, one can begin to start analyzing the slide/slump processes that comprise the MTD.

Slide/slump

The transverse view (Figure 12) shows a northwest–southeast-trending cross section and provides an insight into the internal architecture of the MTD. Toward the compressional regime of the MTD, the seismic reflectors are chaotic and show the sediments slumping on top of each other forming a duplex structure with a series of imbricate thrust faults. The overall sediment direction is interpreted to be coming from the north as the depositional clino-

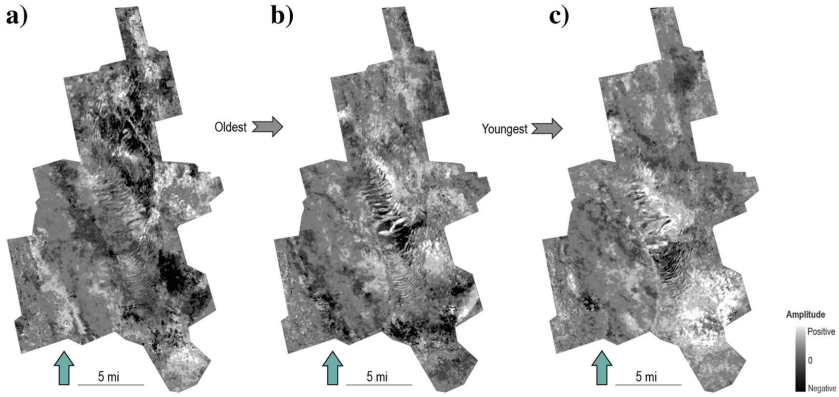

Figure 10. Seismic amplitude values extracted on stratal slices: (a) −1030 ms, (b) −1020 ms, and (c) −1010 ms, showing the change in amplitude anomalies going up the MTD stratigraphic section (left to right). The overall geometry of the MTD is hard to discern using amplitude values only.

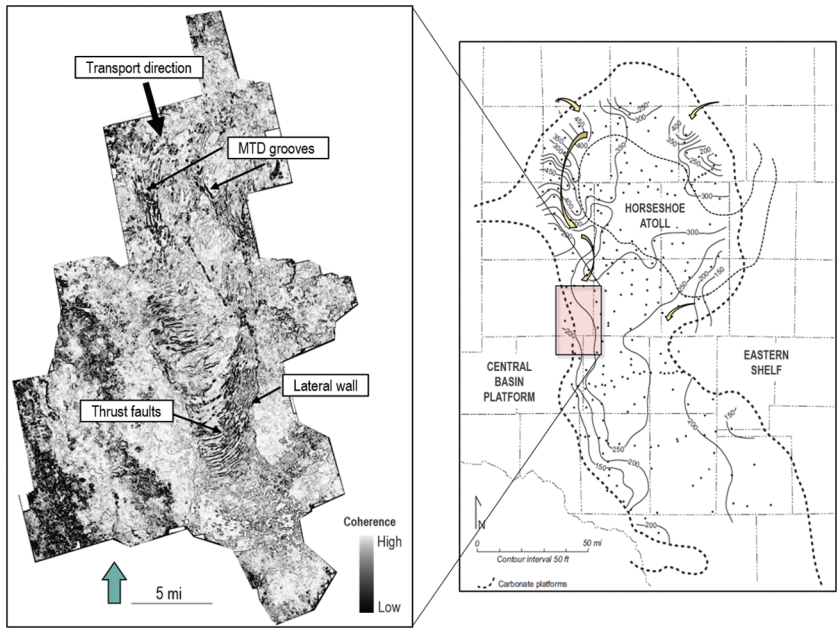

Figure 11. Coherence extracted on a stratal slice showing thrust faults (dipping north–northwest), lateral wall, and overall sediment direction.

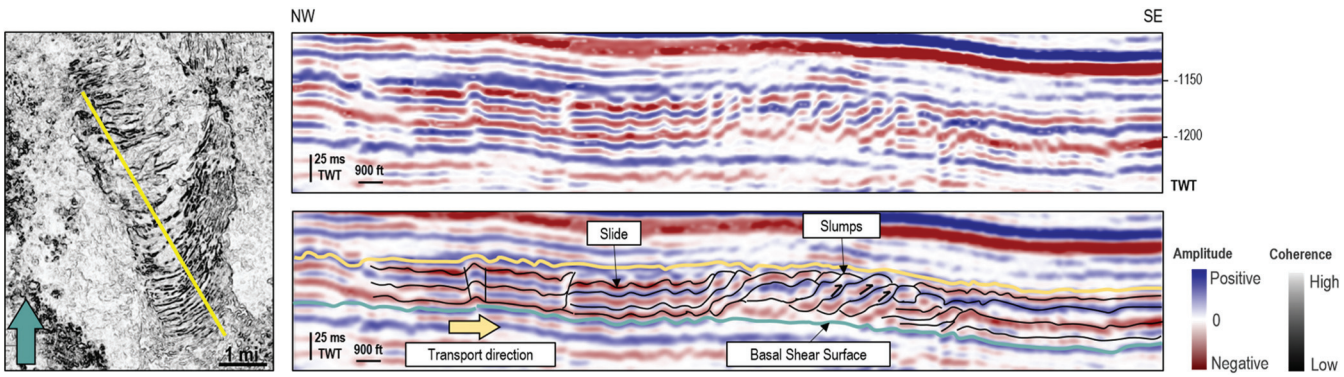

Figure 12. The northwest–southeast seismic cross section showing the internal reflector configuration of the MTD and the interpreted line diagram.

forms (thrust faults) are dipping away from the source. In the southeast portion, the reflectors are less chaotic and lack the abrupt flow of the MTD usually indicated by the presence of the terminal wall. Due to the absence of this terminal wall, it is interpreted that the frontal ramp is buttressed against a topographic high in the Upper Leonard structure in the southeast, eventually slowing the sediments down. The seismic further shows continuous reflectors before the compressional event with little to no internal deformation indicating that the MTD experienced sliding in this section of the event. The wavy relief observed in the sliding portion shows the compressive nature of these flows with localized faulting and detachment folds.

Basal shear surface

The entire MTD event overlies the basal shear surface characterized by much more continuous seismic facies (Figure 12). The basal shear zone represents the plane above which downslope translation occurs. This surface forms the base of the MTD and makes it possible to see where the first MTD succession occurred on seismic. However, depending on the sediment velocity, these flows can sometimes have an erosive nature and can excavate the underlying bathymetry. Identifying the basal shear surface and the top of the MTD reflector (coherent seismic facies, positive amplitude) binds the MTD interval.

Lateral wall

Viewing the reflector configuration from west–east delineates the presence of the lateral wall and its corresponding seismic response (Figure 13). Lateral margins of MTDs are generated parallel to their gross flow direction and can offer a primary kinematic constraint (Bull et al., 2009). This wall can be identified by an obvious change of going from chaotic to coherent seismic reflectors and helps define the lateral extent of the MTD. They are chiefly associated with strike-slip movements in MTDs (Martinsen and Bakken, 1990). As the sediments translate downslope, they are restricted by the presence of this lateral wall, which does not allow the sediments to go past it. As a result, the sediments start shearing in the other direction, eventually slumping on top of each other. On the western margin of the MTD, the underlying bathymetric structure slopes up toward the Central Basin Platform, and the feature is interpreted to stop where the structure begins to climb.

Another observation to be noted is the orientation of the thrust faults within the MTD that can vary considerably as the thrust faults cut through stratigraphic sections as either ramps or flats. In addition, repeated slip on other faults and/or associated folding can cause originally low-angle faults to rotate to steep angles. This is evident in the cross sections (Figure 13a) as the thrust faults dip at high angles buttressed against the lateral wall where the sediments presumably traveled the shortest distance (Posamentier and Martinsen, 2010).

Dip magnitude and azimuth

Dip magnitude and azimuth are reflector configuration attributes and are analogous to the true dip value and dip direction of sedimentary layers. The dip magnitude

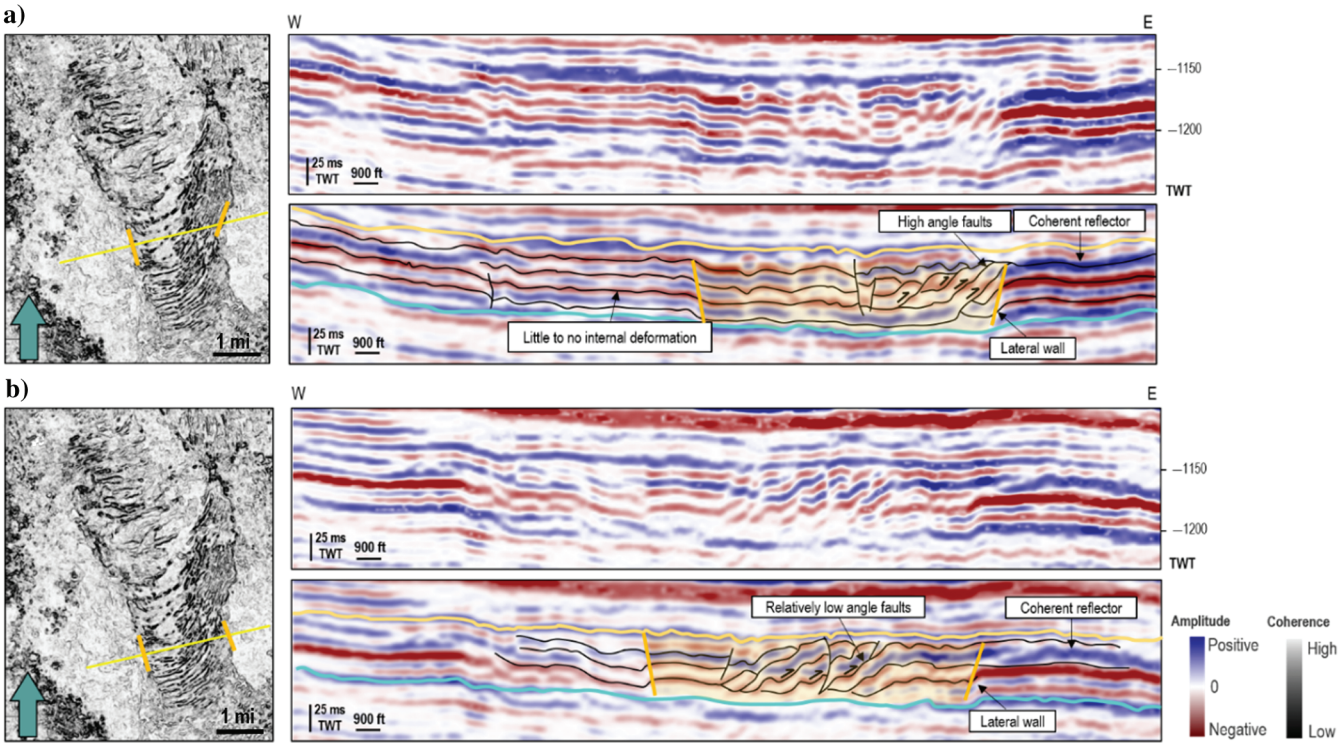

Figure 13. The west–east seismic cross section showing the internal reflector configuration of the MTD and the interpreted line diagram.

(the true dip value) of the reflector can be calculated from the inline and crossline apparent dips. Dip magnitude values range from 0° to 90°. The dip azimuth is the direction of the dip, in which values range from 0° to 360°. There are different ways to estimate dip magnitude and dip azimuth. In this study, we have used Marfurt's (2006) 3D semblance search to estimate the dips. To avoid the misleading dips near fault zones, the semblance search method uses Kuwahara et al.'s (1976) multisearch window method to find the most coherent window.

Dip magnitude and dip azimuth are not only good for mapping structural folds, but also for highlighting subtle faults with very small displacement and understanding the orientation of these faults. In Figure 14, we modify the opacity of dip magnitude such that the corendered image (of the dip azimuth and dip magnitude) highlights the azimuth of only the highly dipping events. The high dip areas are kept transparent and dip azimuth values are visible, whereas the low dip areas are kept opaque and the black color of the dip values does not let the rainbow color of the dip azimuth to be visible. The k_2 strike shows the axis of the fold related to the thrust fault. If we focus on a single thrust fault, we can notice that the fold axis changes with the location. Close to the western end of the thrust fault, the fold axis is nearly west–east, whereas it changes to northeast–southwest in the middle and becomes north-northeast–south-southwest. The dip azimuth also indicates that the strata dip toward north close to the western edge and as we move toward the east, the dip azimuth changes from north to west. The k_2 strike suggests that the strike of the eastern wall is approximately north-northeast–south-southwest, whereas the dip image suggests that the wall is dipping toward the southwest direction.

The attribute helps bring out structural anomalies (discussed in the "Structural curvature" section) that were otherwise not picked by coherence. The dip magnitude and azimuth is a very useful attribute to map the varying orientation of the thrust faults toward the slumping event. This can be helpful in understanding wellbore placement if needed to complete in the MTD zone.

Structural curvature

Structural attributes include the traditional time-structure map, dip azimuth, dip magnitude, and structural curvature, among others (Marfurt, 2018). The attribute measures the curvedness of the bending and folding of seismic reflectors by taking the derivative of the dip in the inline and crossline directions. When viewing geologic features in a 3D environment, curvature is subdivided into the most positive principal curvature (k_1) that shows an anomaly around the peak of the anticline, and the most negative principal curvature (k_2) that shows an anomaly around the trough of the syncline. Figure 15 presents a visual of how the algorithm works for a given fault trace to delineate the peaks and troughs of the thrust fault within the MTD.

Although curvature and coherence are useful in delineating faults, they are not redundant attributes but instead are complementary. In general, coherence, most positive-curvature, and most negative-curvature anomalies often do not align with each other (Marfurt, 2018). For the thrust faults within the MTD, low-coherence anomalies are usually aligned along the fault plane, positive-curvature anomalies are shifted toward the hanging wall, and negative-curvature anomalies are shifted toward the footwall, thereby bracketing the fault trace.

Figure 16 shows how the anomalies map out once this attribute is applied on the MTD stratal slice. The k_2 anomalies (the blue color) highlight the footwall, whereas the k_1 anomalies (the red color) highlight

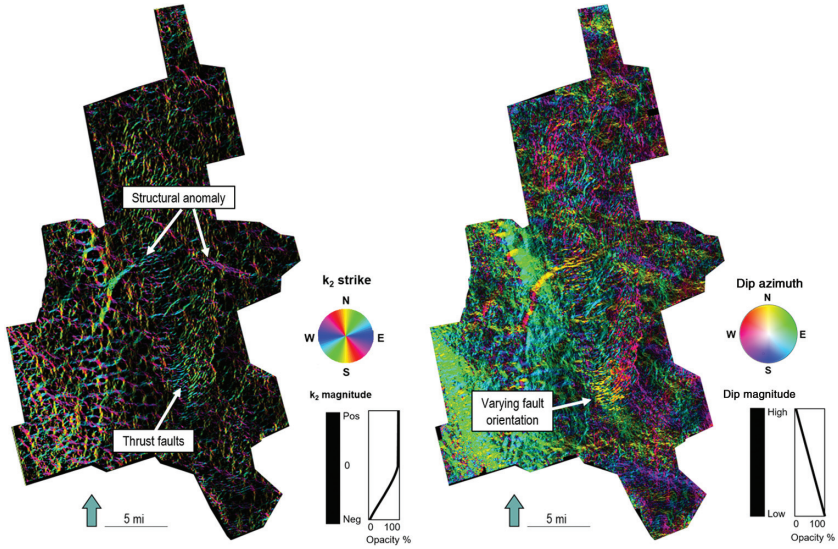

Figure 14. Interpretation of the dip azimuth and dip magnitude and k_2 strike and magnitude. Notice how the orientation of the thrust faults changes within the slumping event.

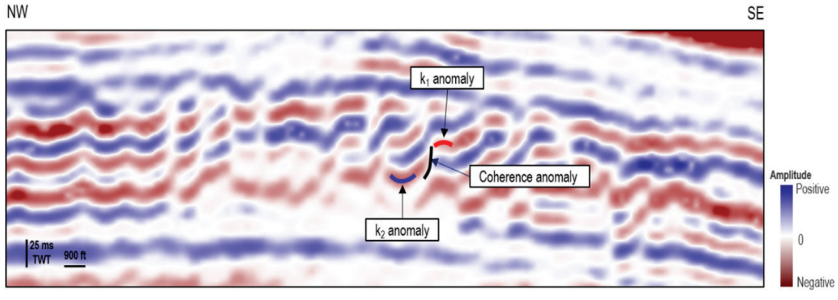

Figure 15. The northwest–southeast cross section illustrating how coherence, k_1, and k_2 anomalies are mapped on the thrust faults.

the hanging wall of these thrust faults. A unique feature stands out (also picked by the dip magnitude and azimuth), which comes off of the Central Basin Platform. This curved "arm" shows up as a strong k_1 and k_2 anomaly. Although coherence does a great job in delineating the overall shape of the MTD, it fails to highlight this curved geometry. This anomaly is due to a deep-seated Paleozoic fault, and as the sediments conformed on top of this structure, it resulted in a bend in the stratigraphic section. The curvature attribute picks this bend in the structure. Coherence does not pick this anomaly because the reflector is continuous and exhibits similar waveform and amplitude values along the dip. The presence of this curved arm is interpreted to have some influence on the seabed topography, overall kinematics of the sediment flow, and the shape of the MTD.

Another anomaly that was picked by the curvature attribute and observed within the MTD body is the presence of discontinuous localized events before the compressional regime that is represented by a strong k_2 anomaly (Figure 16c). These peculiar features trend orthogonal to the overall sediment flow and represent a sedimentary flow that is not related to thrust faulting. The phenomenon that causes this effect is referred to as gravity spreading.

Gravity spreading

Gravity-driven deformations have been widely documented in salt and ice-related compressional deformation (e.g., Anderson et al., 2005; Vendeville, 2005), which results either from gravity gliding or gravity spreading. Gravity spreading is the vertical collapse and spreading of a wedge under its own weight, as opposed to gravity sliding, which is defined as the downslope translation of a body. The key controls for gravity spreading are the dip of the upper surface, the friction along the detachment, and the internal strength of the wedge of sliding material (Rowan et al., 2004). In the case of the MTD in our study area, at some point the mass transport body distorted under its own weight and the sediments started spreading out under the influence of gravity. This left an impression of "V"-shaped scour marks that is observed in seismic and highlighted by strong k_2 anomalies (Figure 17).

Lithologic character of the MTD in the Midland Basin

Mass movements have the potential to move vast amounts of sediment from shelf/slope to deepwater settings and alter the original stratification and lithologic compositions. Such modifications can increase lithologic complexity and can be critical for hydrocarbon exploration. One way to understand the complexity within the MTD is through the use of wireline logs.

Asmus and Grammer (2013) provide an insight on the MTDs response on image logs and conventional logs in the Upper Bone Spring Formation (Upper Leonard) of the Delaware Basin. According to the study, a direct correlation of cores to image logs reveals that MTDs can be identified directly from image logs resulting in contrasting resistivity patterns. The study correlated a sharp decrease in the gamma-ray response for these deposits, indicating an increase in limestone. For the same gamma-ray response, resistivity logs exhibited a sharp increase, which

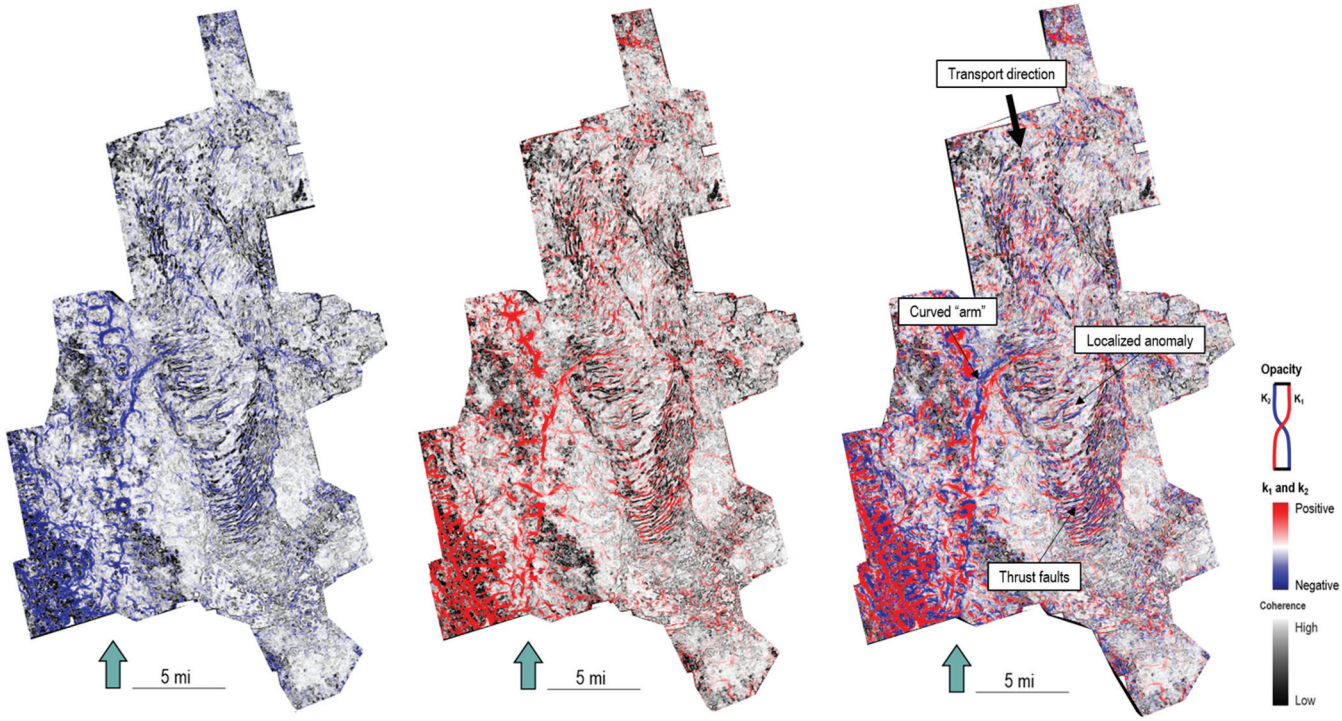

Figure 16. (a) Corendered image of coherence with the k_2 anomaly, (b) corendered image of coherence with the k_1 anomaly, and (c) corendered image of coherence with the k_1 and k_2 anomalies. Notice the localized k_2 anomaly behind the compressional event.

corresponds to a moderate- to high-resistivity (skeletal-rich) response on the image logs.

In the study area, three wells were analyzed using gamma-ray and resistivity logs to understand the lithologic character of the MTD. Figure 18 shows a cross section highlighting wells X and Y that covers the compressional regime of the MTD and well Z that is located outside the MTD. The low gamma-ray and high density (~2.7 g/cm^3) indicates limestone (calcareous lithofacies), whereas a high-gammaray and lower density (<2.65 g/cm^3) response is interpreted as shales (siliciclastic lithofacies). Hence, wells X and Y indicate a mixture of calcareous and siliciclastic sediments and make up the lithologic composition of the 350 ft thick MTD. The porosity logs provide additional information about rock properties. Calcareous rocks typically have higher densities and faster sonic traveltime than siliciclastic sediments. A large separation between the density and neutron porosity curves indicate clay-rich rocks, and a low separation indicates a tighter rock with less porosity.

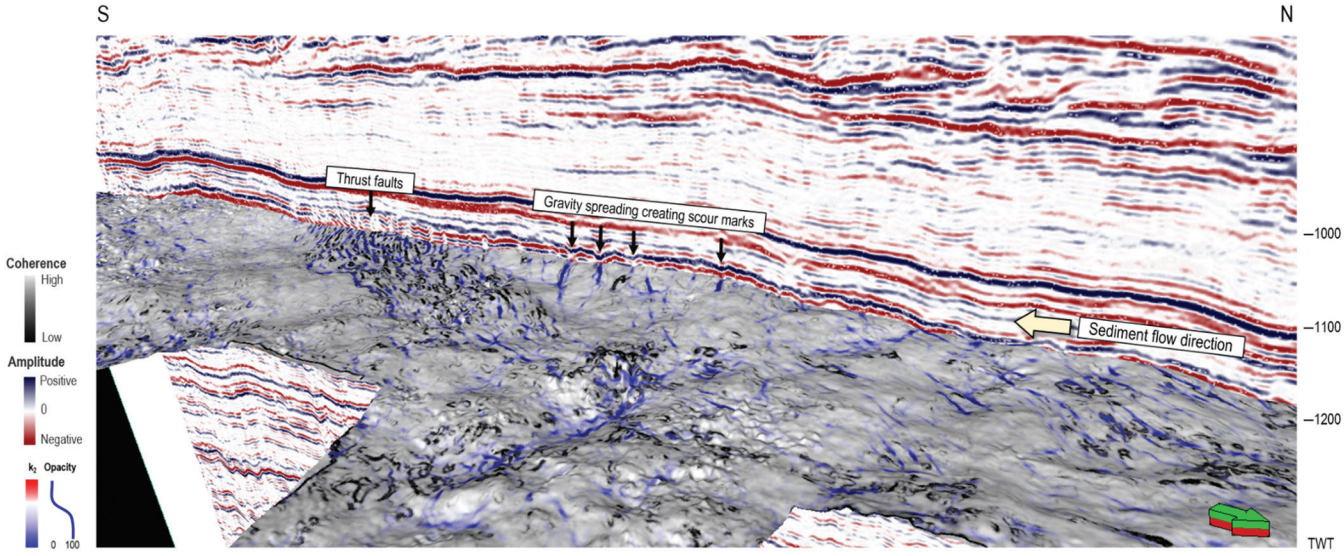

Figure 17. Top of the MTD surface corendered with the coherence and k_2 anomalies highlighting the thrust faults and V-shaped scour marks. The overall sediment direction is interpreted to be coming in from the north.

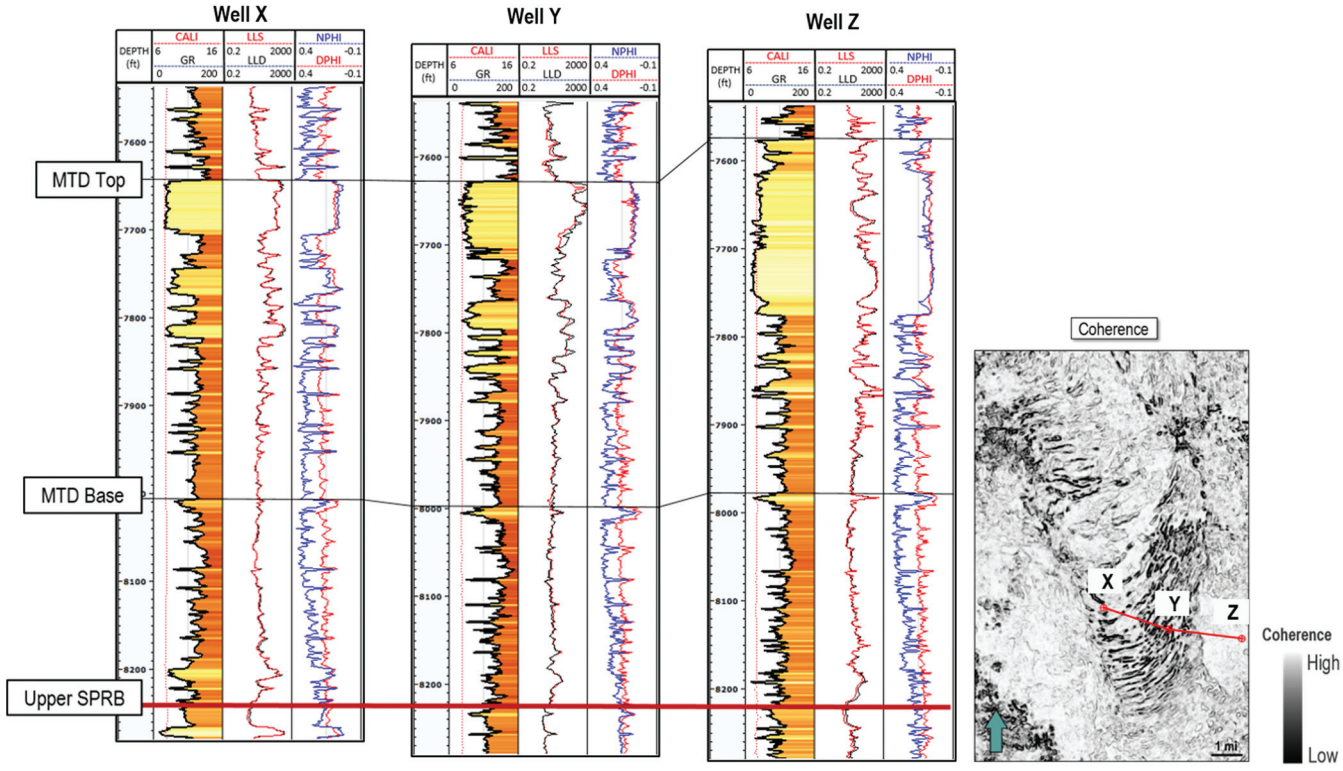

Figure 18. The 350 ft MTD mapped in the Midland Basin consists of a mixture of calcareous and siliciclastic sediments.

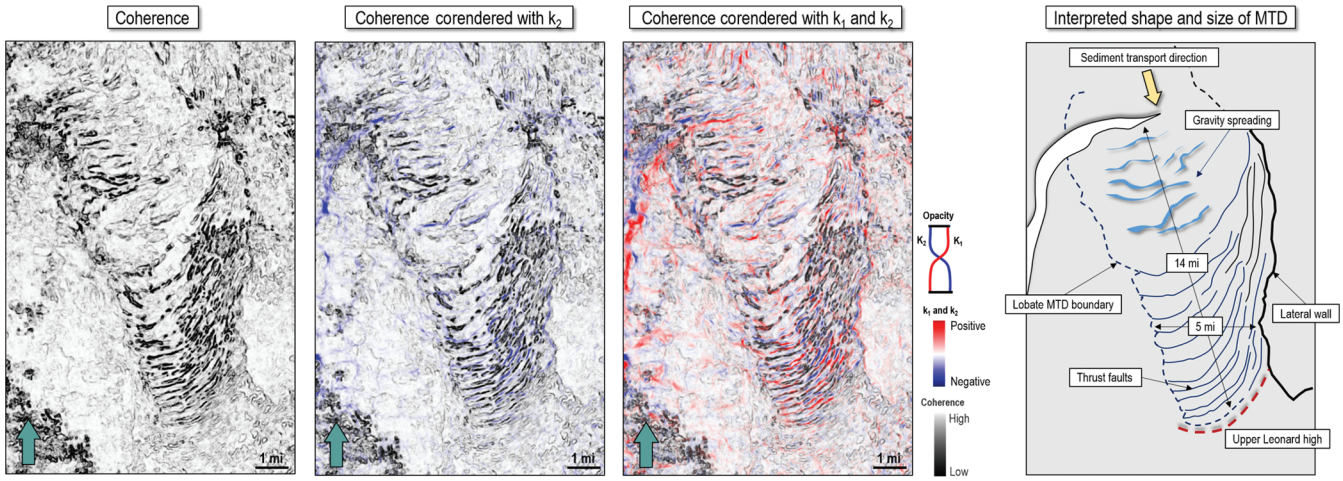

Figure 19. Overall interpretation of the Upper Leonard MTD observed in the Midland Basin. The "curved" arm is a wrench fault (Paleozoic in age) coming off of the Central Basin Platform, and it is interpreted to have some influence on the seabed topography during MTD flow.

Well Z shows a higher concentration of calcareous sediments within the MTD interval with low gamma-ray/high resistivity response, which is interpreted as the slope carbonates of the Central Basin Platform.

Discussion

The 400 mi^2 merged seismic survey allowed observations of how sedimentary features flow during mass transports and the resulting sediment deposition. Geometric attributes (Figure 19) help delineate the structural morphology of the sedimentary flow and sediment flow direction. Three driving forces possibly responsible for the origin of the compressional structures are gravity, compressional stress resulting from rear-push, and shear stress resulting from friction. Previous studies conducted in the Delaware Basin of the Bone Spring Formation (Upper Leonardian) suggest that shelf edge and slope deposition of sediments occurred as a result of decreased accommodation space due to increased carbonate production and over-steeping of a vertically aggrading shelf margin (Wiggins and Harris, 1985; Gawloski, 1987; Saller et al., 1989). In the case of the MTD in the Midland Basin, the mechanism that triggered this sedimentary flow is still unknown and is open to interpretation. A study (Allen et al., 2013) conducted in the Delaware Basin demonstrated that MTDs can enhance production if targeted optimally where the faults enhance production rather than restrict it. This study investigated that the first well drilled inside the MTD zone of the second Bone Spring sand had a 30 day average IP of 835 BOPD, which greatly outperformed the average second Bone Spring well of 344 BOPD located outside the MTD.

Conclusion

MTDs observed in the Permian Basin are widespread deposits and can extend up to several miles. The MTD mapped in the study area covers the translational and compressional regime of the mass movement. Kinematic evidence provided by the upper Spraberry isopach suggests the MTD flow direction was from the north toward bathyal depths as the sediments followed the peak and saddle morphology of the Horseshoe Atoll before settling down. Sobel filter-based coherence along with curvature attributes help map thrust faults, lateral walls, and the localized anomalies observed within the MTD. The k_2 anomaly that highlights the footwall of the thrust faults is the same k_2 anomaly that highlights the V-shaped scour marks at the upper MTD body due to gravity spreading. The curved arm (wrench fault) coming off the Central Basin Platform is interpreted as a bend in the structure that is affected by a deep-seated Paleozoic fault. This may have acted as a constraint on the internal kinematics, seabed topography, and the shape and size of the MTD.

The 350 ft thick MTD lithology is composed of carbonates and shales with a moderate- to high-resistivity response and agrees with wireline correlations of the cyclic Leonardian platform deposits prograding toward the basin from clinoformal carbonates into flat-lying calcareous and siliciclastic intervals. Based on reports from the zone of study and its location in the depositional system, the reservoir potential for the MTD looks promising in the Midland Basin. In terms of understanding connectivity issues due to thrust faulting, fracability of the flow and/or compartmentalization of the reservoir is a topic for future research.

Acknowledgments

We would like to thank Fasken Oil and Ranch for the 3D seismic survey and well log donation to the UT Permian Basin. We thank M. Scipione and T. Tittlemier from Trey Resources for their insightful advice and stimulating discussions throughout the research experience. We used Attribute Assisted Seismic Processing and Interpretation Consortium's AASPI software to compute seismic attributes. We used Schlumberger's Petrel for 3D seismic visualization and interpretation and TechLog for well-log correlation.

Data and materials availability

Data associated with this research are confidential and cannot be released.

References

Adiletta, S., R. Holt, A. Kaba, L. Gimenez, K. Koster, and N. Coevering, 2019, The role of geophysics in Oxy's Permian Basin unconventional resource play appraisal and development workflow: First Break, **37**, 45–52.

Allen, J., K. Schwartz, J. DeSantis, D. Koglin, and F. Chen, 2013, Integration of structure and stratigraphy in Bone Spring tight oil sandstones using 3D seismic in the Delaware Basin, TX: 1st Unconventional Resources Technology Annual Conference, URTEC-1619830-MS, 2521-2527, doi: 10.1190/urtec2013-262.

Amerman, R., 2009, Deepwater mass-transport deposits: Structure, stratigraphy, and implications for basin evolution: Ph.D. dissertation, Colorado School of Mines, doi: 10.13140/RG.2.1.1873Paul7687.

Anderson, L. T., D. L. Hansen, and M. Huuse, 2005, Numerical modelling of thrust structures in unconsolidated sediments: Implications for glaciotectonic deformation: Journal of Structural Geology, **27**, 587–596, doi: 10.1016/j.jsg.2005.01.005.

Asmus, J. J., and G. M. Grammer, 2013, Characterization of deepwater carbonate turbidites and mass-transport deposits utilizing high-resolution electrical borehole image logs: Upper Leonardian (Lower Permian) Upper Bone Spring Limestone, Delaware Basin, Southeast New Mexico and West Texas: Gulf Coast Association of Geological Societies Transactions, **63**, 27–65.

Bhatnagar, P., 2018, Geomorphologic character of an Upper Leonardian mass transport deposit, Midland Basin: Insights from 3D seismic data: M.S. thesis, UT Permian Basin.

Bull, S., J. Cartwright, and M. Huuse, 2009, A review of kinematic indicators from mass transport complexes using 3D seismic data: Marine and Petroleum Geology, **26**, 1132–1151, doi: 10.1016/j.marpetgeo.2008.09.011.

Dingle, R. V., 1977, The anatomy of a large submarine slump on a sheared continental margin (SE Africa): Journal of the Geological Society, **134**, 293–310, doi: 10.1144/gsjgs.134.3.0293.

Festa, A., K. Ogata, G. A. Pini, Y. Dilek, and J. L. Alonso, 2016, Origin and significance of olistostromes in the evolution of orogenic belts: A global synthesis: Gondwana Research, **39**, 180–203, doi: 10.1016/j.gr.2016.08.002.

Gawloski, T. F., 1987, Nature, distribution, and petroleum potential of Bone Spring detrital sediments along the Northwest Shelf of the Delaware Basin, *in* D. Cromwell and L. Mazzullo, eds., The Leonardian facies in West Texas and Southeast New Mexico and guidebook to the Glass Mountains, West Texas: Permian Basin Section of the Society of Economic Paleontologists and Mineralogists, 85–106.

Hamlin, H. S., and R. W. Baumgardner, 2013, Wolfberry (Wolfcampian-Leonardian) deep-water depositional systems in the Midland Basin: Stratigraphy, lithofacies, reservoirs, and source rocks: Bureau of Economic Geology.

Handford, C. R., 1981a, Deep-water facies of the Spraberry Formation (Permian), Reagan County, Texas, *in* C. T. Siemers, R. W. Tillman, and C. R. Williamson, eds., Deep-water clastic sediments — A core workshop: Society of Economic Paleontologists and Mineralogists, 372–395.

Handford, C. R., 1981b, Sedimentology and genetic stratigraphy of Dean and Spraberry Formations (Permian), Midland Basin, Texas: AAPG Bulletin, **65**, 1602–1616.

Hoak, T., K. Sundberg, and P. Ortoleva, 1998, Overview of the structural geology and tectonics of the Central Basin Platform, Delaware Basin, and Midland Basin, West Texas and New Mexico: Science Applications International Corporation.

Kelly, L., J. Bachmann, D. Amoss, B. Angelico, B. Corales, B. Fernandez, P. Kissel, R. Roberts, and H. Stewart, 2012, Permian Basin: Easy to oversimplify, hard to overlook: Exploration and Production Journal, Howard Weil, 1–46.

Kuwahara, M., K. Hachimura, S. Eiho, and M. Kinoshita, 1976, Digital processing of biomedical images: Plenum Press, 187–203.

Lewis, K. B., 1971, Slumping on continental slope inclined at 1–4°: Sedimentology, **16**, 97–110, doi: 10.1111/j.1365-3091.1971.tb00221.x.

Marfurt, K. J., 2006, Robust estimates of 3D reflector dip and azimuth: Geophysics, **71**, no. 4, P29–P40, doi: 10.1190/1.2213049.

Marfurt, K. J., 2018, Seismic attributes as the framework for data integration throughout the oilfield life cycle: SEG.

Martinez, F. J., 2010, 3D seismic interpretation of mass transport deposits: Implications for basin analysis and geohazard evaluation, *in* D. C. Mosher, C. Shipp, L. Moscardelli, J. Chaytor, C. Baxter, H. Lee, and R. Urgeles, eds., Submarine mass movements and their consequences. Advances in natural and technological hazards research: Springer 553–568.

Martinsen, O. J., 1994, Mass movements, *in* A. Maltman, ed., The geological deformation of sediments: Chapman and Hall, 127–165.

Martinsen, O. J., and B. Bakken, 1990, Extensional and compressional zones in slumps and slides in the Namurian of County Clare, Eire: Journal of Geological Society, **147**, 153–164, doi: 10.1144/gsjgs.147.1.0153.

Moscardelli, L., L. Wood, and P. Mann, 2006, Mass-transport complexes and associated processes in the offshore area of Trinidad and Venezuela: AAPG Bulletin, **90**, 1059–1088, doi: 10.1306/02210605052.

Nissen, S. E., N. L. Haskell, C. T. Steiner, and K. L. Coterill, 1999, Debris flow outrunner blocks, glide tracks, and pressure ridges identified on the Nigerian continental slope using 3-D seismic coherency: The Leading Edge, **18**, 595–599, doi: 10.1190/1.1438343.

Posamentier, H. W., 2017, Seismic stratigraphy and geomorphology — The next frontier 21st century reservoir

characterization: South West Section (SWS) Bill Hailey short course: AAPG.
Posamentier, H. W., and V. Kolla, 2003, Seismic geomorphology and stratigraphy of depositional elements in deep-water settings: Journal of Sedimentary Research, **73**, 367–388, doi: 10.1306/111302730367.
Posamentier, H. W., and O. J. Martinsen, 2010, The character and genesis of submarine mass-transport deposits: Insights from outcrop 3D seismic data, *in* R. C. Shipp, P. Weimer, and H. W. Posamentier, eds., Mass-transport deposits in deepwater settings: Society for Sedimentary Geology 7–38.
Posamentier, H. W., and R. G. Walker, 2006, Deep-water turbidites and submarine fans, *in* H. W. Posamentier and R. G. Walker, eds., Facies models revisited: SEPM 84, 397–520.
Posamentier, H. W., P. S. Wisman, and T. Plawman, 2000, Deep water Meizarwin depositional systems — Ultradeep Makassar Strait, Indonesia, *in* P. Weimer, ed., Deep water reservoirs of the World: Gulf Coast Section SEPM Foundation, 806–816.
Qi, J., F. Li, and K. J. Marfurt, 2017, Multiazimuth coherence: Geophysics, **82**, no. 6, O83–O89, doi: 10.1190/geo2017-0196.1.
Rowan, M. G., F. J. Peel, and B. C. Vendeville, 2004, Gravity driven fold belts on passive margins, *in* K. R. McClay, ed., Thrust tectonics and hydrocarbon systems: AAPG Memoir 82, 157–182.
Ruppel, S. C., W. B. Ward, E. E. Ariza, and J. W. Jennings, 2000, Cycle and sequence stratigraphy of Clear Fork reservoir-equivalent outcrops: Victorio Peak Formation, Sierra Diablo, Texas, *in* R. F. Lindsay, R. F. Ward, R. C. Trentham, and A. H. Smith, eds., Classic Permian geology of West Texas and southeastern New Mexico, 75 years of Permian Basin oil & gas exploration and development: West Texas Geological Society, 109–130.
Saller, A. H., J. W. Barton, and R. E. Barton, 1989, Slope sedimentation associated with a vertically building shelf, Bone Spring Formation, Mescalero Escarpe Field, southeastern New Mexico, *in* P. D. Crevello, J. L. Wilson, J. F. Sarg, and J. F. Read, eds., Controls on carbonate platform and basin development: Society of Economic Paleontologists and Mineralogists 44, 275–288.
Shipp, R. C., P. Weimer, and H. W. Posamentier, 2011, Mass-transport deposits in deepwater settings: An introduction, *in* R. C. Shipp, P. Weimer, and H. W. Posamentier, eds., Mass-transport deposits in deepwater settings: SEPM Society for Sedimentary Geology 96.
Vendeville, B. C., 2005, Salt tectonics driven by sediment progradation — Part 1: Mechanics and kinematics: AAPG Bulletin, **89**, 1071–1079, doi: 10.1306/03310503063.
Verma, S., Y. Del Moro, and K. J. Marfurt, 2013, Pitfalls in prestack inversion of merged seismic surveys: Interpretation, **1**, no. 1, A1–A9, doi: 10.1190/INT-2013-0024.1.
Vest, E. L., 1970, Oil fields of Pennsylvanian-Permian Horseshoe Atoll, West Texas, *in* M. T. Halbouty, ed., Geology of giant petroleum fields: AAPG Memoir 14, 185–203.
Wiggins, W. D., and P. M. Harris, 1985, Burial diagenetic sequence in deep-water allochthonous dolomites: Permian Bone Spring Formation, Southeast New Mexico: Society of Economic Paleontologists and Mineralogists Core Workshop, 6, 140–173.

Paritosh Bhatnagar received a bachelor's degree in physics from Angelo State University and a master's degree in geophysics from The University of Texas of the Permian Basin. He worked at Trey Resources for two years analyzing their Alpine High acreage as a geophysicist. He is currently employed at Ikon Science as a technical geoscientist with a focus on rock physics, inversion, and geomechanics in unconventional reservoirs.

Sumit Verma received an M.S. (2007) in applied geophysics from the Indian School of Mines, Dhanbad, and a Ph.D. (2015) in geophysics from the University of Oklahoma under the supervision of Kurt Marfurt. After receiving a Ph.D., he worked for one year as a postdoctoral research fellow at the University of Wyoming. He is an assistant professor of geophysics at UTPB and became acting chair of the Department of Geosciences in 2019. He also worked with Reliance Industries Ltd. E&P for four years (2007–2011) as a development geoscientist. His scientific writing includes 15 technical papers in well-known geoscience journals and more than 40 abstracts. He is a deputy associate editor for the peer-reviewed scientific journal *Interpretation*. His research interests include seismic interpretation, quantitative interpretation, and reservoir characterization.

Ron Bianco received a B.S. and an M.S. in geophysics from Texas A&M University, where he specialized in numerical modeling of the effects of fluid on the stability of fault gouge materials. He began his career at Apache Corporation prospecting for oil and gas wells in multiple basins including the Gulf of Mexico shelf, South Texas Eagle Ford, and the Permian Basin. He is currently the senior staff geophysicist for Fasken Oil & Ranch, where he continues his work on exploration and exploitation in fields across North America. He is also the president and cofounder of the Iron Freedom Foundation, a nonprofit 501(c)(3) for returning combat veterans, which provides support and outfits veterans with the tools they need to be successful in civilian life.